$NaNbO_3:Pr^{3+}$: a new red phosphor showing persistent luminescence

2009 J. Phys.: Condens. Matter 21 025901

(http://iopscience.iop.org/0953-8984/21/2/025901)

J. Phys.: Condens. Matter **21** (2009) 025901 (6pp) doi:10.1088/0953-8984/21/2/025901

$NaNbO_3:Pr^{3+}$: a new red phosphor showing persistent luminescence

P Boutinaud[1], **L Sarakha and R Mahiou**

Clermont Université, Université Blaise-Pascal, Laboratoire des Matériaux Inorganiques, UMR CNRS 6002, Ensemble Scientifique des Cézeaux, 63177 Aubière, France

E-mail: Philippe.Boutinaud@univ-bpclermont.fr

Received 16 July 2008, in final form 20 October 2008
Published 9 December 2008
Online at stacks.iop.org/JPhysCM/21/025901

Abstract

The Pr^{3+}-doped $NaNbO_3$ perovskite is introduced as a new red phosphor excitable in the near UV region at around 350 nm. A bright single red emission is observed at room temperature and ascribed to transitions between the $^1D_2$ excited state and the ground state $^3H_4$ of Pr^{3+} ions. This peculiar behavior is related to the presence of a low-lying intervalence charge transfer state that contributes to quench the emission from the otherwise emitting $^3P_0$ level. Red afterglow is also evidenced in $NaNbO_3:Pr^{3+}$. A preliminary model is discussed to clarify the afterglow mechanism.

1. Introduction

In the past years, a systematic investigation of Pr^{3+}-doped oxide-based lattices, incorporating closed shell transition metal groups, has led to a model which explains the particular luminescence properties of these materials. The model is based on the formation of a metal-to-metal intervalence charge transfer state (IVCT) that was shown to interfere with the excited states dynamics of the Pr^{3+} ion by providing an efficient quenching channel by cross-over to the $^3P_0$ level and in a few cases to the $^1D_2$ level [1–5].

A preliminary equation (1) connecting the experimental energy position of the IVCT observed on excitation spectra to the optical electronegativity ($\chi_{opt}(M^{n+})$) of the d^0 metal cation $M^{n+} = Ti^{4+}$, V^{5+}, Nb^{5+}, Ta^{5+} and the shortest Pr^{3+}–M^{n+} distance $d(Pr^{3+}–M^{n+})$ in the host structure has been formulated [5]. This empirical equation has the form

$$\mathrm{IVCT}(Pr^{3+},\ \mathrm{cm}^{-1}) = 58\,800 - 49\,800\frac{\chi_{\mathrm{opt}}\left(M^{n+}\right)}{d(Pr^{3+}–M^{n+})}. \quad (1)$$

This equation allows the location of the IVCT state in a given host within ± 1500 cm^{-1} from its known structural features.

Additionally, this equation may serve as a predictive tool for the design of red emitting compounds doped with Pr^{3+}. In particular, the IVCT mechanism allows specific tailoring of the photoluminescence for applications requiring low energy excitation or pure color outputs (i.e. down-conversion phosphors for photovoltaic purposes or phosphors excited by near UV LED chips).

The Pr^{3+}-doped perovskite $NaNbO_3$, whose luminescence properties have not yet been described, is one representative example of this approach. In this paper, we propose to investigate the luminescence and afterglow properties of $NaNbO_3:Pr^{3+}$ in the light of the IVCT model.

In order to achieve better understanding of the afterglow mechanisms in $NaNbO_3:Pr^{3+}$ a parallel is made with two well known compounds: $CaTiO_3:Pr^{3+}$, whose luminescence properties obey equation (1) and for which persistent luminescence has been demonstrated [6–12], and $LiNbO_3:Pr^{3+}$, that also glows in the red spectral region [13] but shows no persistent luminescence at any temperature.

2. Experimental details

$NaNbO_3:Pr^{3+}$ and $LiNbO_3:Pr^{3+}$ polycrystalline samples were prepared by routine solid state reaction involving typically a heat treatment for 6 h at 1200 °C under air. The reagents were sodium or lithium carbonates, Nb_2O_5 and Pr_6O_{11}. The nominal doping rate was 0.1 mol%. No charge compensation was achieved.

The powders were carefully checked to be single phased by x-ray diffraction. The diffraction patterns matched the JCPDS powder diffraction cards 33-1270 for $NaNbO_3$ and 20-631 for $LiNbO_3$. $LiNbO_3$ is a superstructure of corundum with

[1] Author to whom any correspondence should be addressed.

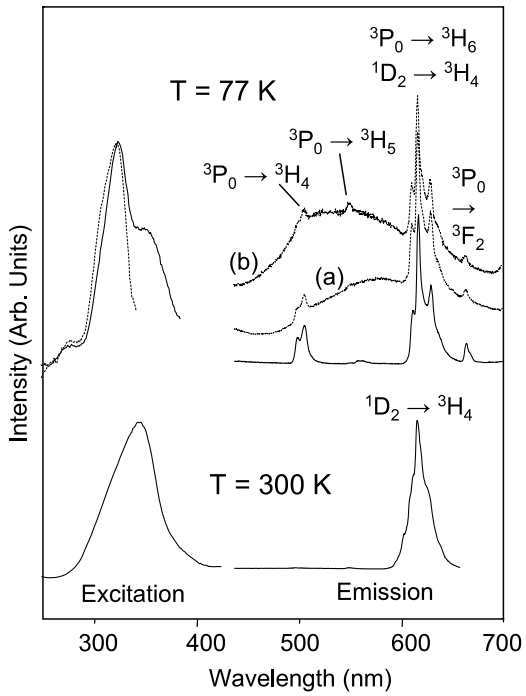

Figure 1. Steady state luminescence spectra of $NaNbO_3$:Pr^{3+}. The excitation spectra (left) in solid and dotted lines were monitored at $\lambda_{em} = 620$ and 570 nm, respectively. The emission spectra (right) in solid lines were recorded upon excitation at $\lambda_{exc} = 350$ nm. Emission spectra in dotted lines were measured for $\lambda_{exc} = 320$ nm (a) or $\lambda_{exc} = 300$ nm (b).

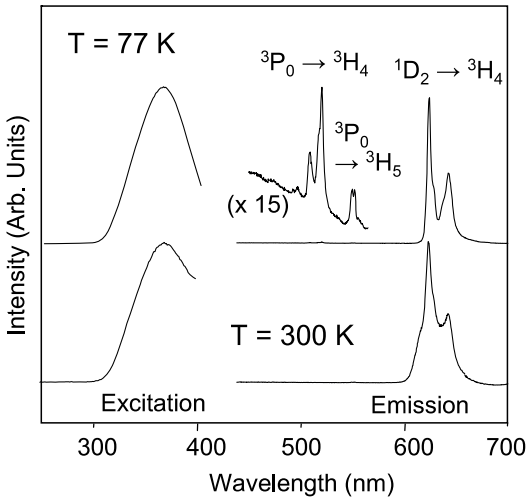

Figure 2. Steady state luminescence spectra of $LiNbO_3$:Pr^{3+}. The excitation spectra (left) were monitored at $\lambda_{em} = 620$ nm. The emission spectra (right) were recorded upon excitation at $\lambda_{exc} = 350$ nm.

the rhombohedral space group $R\bar{3}c$. It is expected that the Pr^{3+} ions enter the octahedrally coordinated Li^+ sites, which have nominally C_3 point symmetry since the Li^+ ions occupy an off-centered position [14]. The average Li–O distance in the octahedron is 2.15 Å and the shortest Li^+–Nb^{5+} distance in $LiNbO_3$ is 3.05 Å. This distance is even expected to be slightly lowered after substitution of Li^+ to Pr^{3+} due to the ionic size mismatch.

Sodium niobate is one of the more complex perovskite materials as it shows up to six phase transitions from the low temperature ferroelectric phase of space group $R\bar{3}c$ to the high temperature paraelectric cubic phase with space group $Pm3m$, through different antiferroelectric and paraelectric phases of other symmetries [15].

At room temperature, $NaNbO_3$ is orthorhombic with the space group normally considered as $Pbma$. Two sodium sites are present in the structure. The coordination number is 12 for both sites but with Na–O distances ranging from 2.499 to 3.282 Å in one of the sites and from 2.303 to 3.188 Å in the second site, giving an average Na–O distance of 2.77 Å in both cases. The shortest Na^+–Nb^{5+} distance in $NaNbO_3$ is 3.29–3.30 Å, depending on the considered site. This distance should not be significantly affected by the substitution of Na^+ to Pr^{3+} since both ions have very similar ionic radii.

It is worthwhile noting the similarity existing between the $LiNbO_3$ and the perovskite structure [16], both structures consisting of corner shared niobate octahedra. However, one significant difference between the two structures is that the maximum Nb–O–Nb angle between shared octahedra increases from 140° in $LiNbO_3$ to about 160° in $NaNbO_3$. In addition, in the latter case, up to four angles are found in the range 153°–164° against only one angle at 140° in the former case (the others being lower).

The photoluminescence and afterglow spectra were collected using a continuous wave monochromatized xenon lamp as excitation source (TRIAX 180 from Jobin-Yvon/Horiba) and a TRIAX 550 Jobin-Yvon/Horiba monochromator equipped with either a R928 Hamamatsu photomultiplier or a nitrogen-cooled CCD camera as detector.

The afterglow emission spectra were recorded after irradiation of the samples for 1 min at 350 nm. Each spectrum was acquired during 1 s and the delay between two successive spectra was 2 s. A first emission spectrum was recorded upon irradiation (not shown in the figures) and the incoming beam was switched off 1 s before the recording of the first afterglow spectrum. All the afterglow spectra were collected using the same experimental conditions and are displayed on the same intensity scale.

The high temperature data were acquired with the help of a home-made copper holder heated by a thermocoax wire connected to a Thermolyne regulator. The decay profiles were recorded at 300 and 77 K using a nitrogen laser ($\lambda_{exc} = 337$ nm) and a 400 MHz LeCroy digital oscilloscope with an input impedance of 50 Ω.

3. Results and discussion

3.1. Luminescence and excited state dynamics

Representative steady state photoluminescence spectra of $NaNbO_3$:Pr^{3+} and of $LiNbO_3$:Pr^{3+} are reproduced in figures 1 and 2, respectively. At room temperature, both compounds show single red $^1D_2 \rightarrow {}^3H_4$ emission from the Pr^{3+} ions upon excitation at 350 nm. At 77 K, emission features from

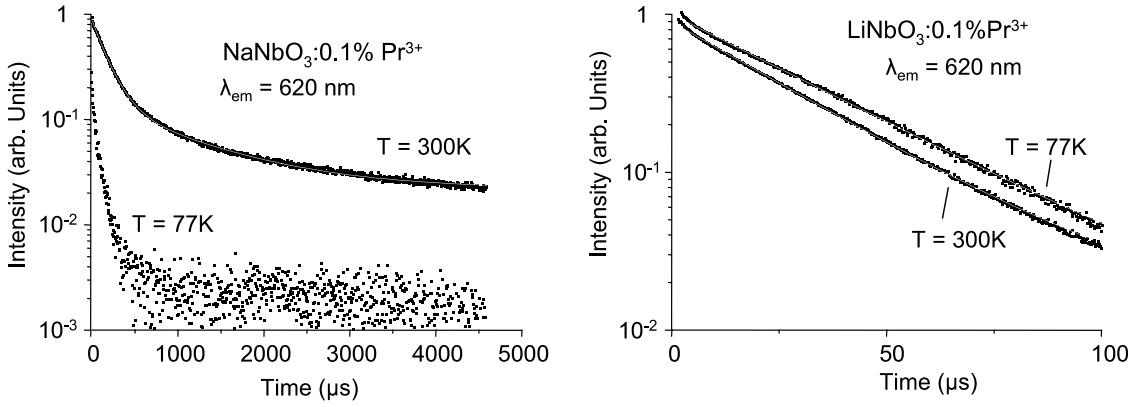

Figure 3. Decay profiles of $NaNbO_3$:Pr^{3+} and $LiNbO_3$:Pr^{3+} excited at 337 nm at different temperatures. The solid line is the fit of the experimental data (see the text).

the $^3P_0$ level are observed in $NaNbO_3$:Pr^{3+} but remain almost indiscernible in $LiNbO_3$:Pr^{3+}. In the latter case, however, a magnification of the spectrum allows the observation of $^3P_0 \rightarrow {}^3H_4$ transitions with principal peaks positioned at 509.9, 518.4 (hump) and 521.2 nm, in fair agreement with data reported in [17].

The excitation spectra related to the red luminescence at room temperature are dominated by a broad band centered at 344 nm (≈29 070 cm^{-1}) and 368 nm (≈27 175 cm^{-1}), respectively in $NaNbO_3$:Pr^{3+} and $LiNbO_3$:Pr^{3+}. In agreement with previous investigations, we ascribe this band to intervalence charge transfer (IVCT) [4, 5, 18].

The intrinsic luminescence properties of undoped lithium and sodium niobates were studied in the 1980s by Blasse and De Haart [19]. At 4.2 K, $LiNbO_3$ is characterized by a broad emission centered at 440 nm with an excitation maximum peaking at 260 nm. This luminescence is suggested to be due to the charge transfer vibronic exciton in the regular oxy-anion site [20]. The Stokes shift of this emission is about 15 700 cm^{-1}. It is characteristic of the intrinsic niobate group having negligible interaction with other nearby niobate groups [19]. In fact, the absorption edge of $LiNbO_3$ is difficult to determine accurately as it is very sensitive to composition. Typical values range from about 300 to 320 nm depending on the Li/Nb ratio [21].

Doping $LiNbO_3$ has also been experienced to induce important shifts of the absorption edge due to a variation of the Li/Nb ratio [22]. For instance, Pr^{3+}-doped $LiNbO_3$ crystals show an absorption edge at about 400 nm (25 000 cm^{-1}) and two excitation bands at 385 and 330 nm (26 000 and 30 300 cm^{-1} respectively) for the red Pr^{3+} luminescence [18, 23]. The lower energy band was ascribed to a trapped exciton state while the band at higher energy was ascribed to the host.

At 4.2 K, $NaNbO_3$ shows two broad emission bands at 480 and 540 nm correlated with excitation maxima at 300 and 320 nm, respectively [19]. The Stokes shift is similar for both of these emissions at about 12 600 cm^{-1}. According to Blasse and De Haart, the decrease of the Stokes shift going from $LiNbO_3$ to $NaNbO_3$ indicates stronger delocalization of the electronic wavefunctions resulting from the increase of the Nb–O–Nb angle.

The excitation spectra for the red luminescence in $LiNbO_3$:Pr^{3+} (see figure 2) do not reveal any intrinsic feature of the niobate host, in contrast to results reported in [18, 23]. This difference is possibly due to saturation effects that occur more efficiently in powdered samples than in transparent single crystals or thin films [12]. It has not been possible to observe any emission feature from the host in $LiNbO_3$:Pr^{3+}, whatever the temperature (for $T \geqslant 77$ K) or the excitation wavelength.

In contrast, the excitation spectra of $NaNbO_3$:Pr^{3+} involve two principal contributions that are clearly resolved at 77 K. At this temperature, the bands are centered respectively at around 325 nm (30 770 cm^{-1}) and 351 nm (28 490 cm^{-1}). The latter band is due to IVCT while the former is assigned to the niobate host.

Exciting at either 325 or 300 nm at 77 K yields the typical niobate emissions of undoped $NaNbO_3$ [19], superimposed on the Pr^{3+} features (see figure 1). At 77 K, the luminescence mechanism in $NaNbO_3$:Pr^{3+} is dominated by host sensitization and the luminescence efficiency of this compound in the red region is low compared to the situation at room temperature. Upon warming to room temperature, the IVCT mechanism becomes prominent and the emission intensity is stronger.

The efficiency of the luminescence quenching in the Pr^{3+}-doped niobates was evaluated by recording the temporal decay profiles of the red emission at either 300 or 77 K, upon excitation at 337 nm. The results, shown in figure 3, clearly indicate that the emission decays are much shorter in $LiNbO_3$:Pr^{3+} than in $NaNbO_3$:Pr^{3+}. For the red emission in $LiNbO_3$:Pr^{3+} (i.e. $^1D_2 \rightarrow {}^3H_4$ transition), the decay is exponential at both temperatures with a time constant varying from 27 μs at 300 K to 31 μs at 77 K. These results are in agreement with [13].

The decay profile of the $^3P_0$ emission is not shown here as it was too short to be measured accurately with our set-up. We note however that a time constant in the range of 0.5 μs has been reported for this level at low temperature in dilute $LiNbO_3$:Pr^{3+} [13, 17], indicating that an efficient radiationless relaxation occurred from this level.

The quenching of the $^3P_0$ emission in $LiNbO_3:Pr^{3+}$ was first ascribed to cross-relaxation [17], then revisited in [18] and finally ascribed to non-radiative relaxation by cross-over between the $^3P_0$ level and a low-lying trapped exciton state. This quenching process is qualitatively very similar to the IVCT quenching model developed in [1–5]. Owing to this model, strong quenching of the $^3P_0$ level can be induced by cross-over to a low-lying charge transfer state formally of the type Pr^{4+}–$M^{(n-1)+}$, where M^{n+} is a transition metal of d^0 configuration.

In $NaNbO_3:Pr^{3+}$, the room temperature decay profile of the red $^1D_2 \rightarrow {}^3H_4$ emission was well reproduced using the double exponential:

$$I(t) = I_1 \exp(-t/\tau_1) + I_2 \exp(-t/\tau_2) \qquad (2)$$

with $\tau_1 = 170\ \mu s$ and $\tau_2 = 1085\ \mu s$. The time constant τ_1 is in the range of usual values observed for the $^1D_2$ level exposed to relatively inefficient radiationless relaxation, for Pr^{3+} ions diluted in oxide-based lattices [13, 24–26]. Much lower values of this lifetime can be measured in more concentrated systems (quenching by cross-relaxation) or by incorporating the Pr^{3+} ion in lattices having high phonon frequency modes like phosphates or borates (quenching by multiphonon relaxation).

The time constant τ_2 is, in contrast, too high to be ascribed to the $^1D_2$ level. This slow component is attributed to a post-luminescence contribution involving the $^1D_2$ level. A very similar behavior was evidenced upon UV irradiation in the case of the red phosphorescent $CaTiO_3:Pr^{3+}$ compound [6, 10, 27].

Decreasing the temperature to 77 K induced a significant shortening of the decay profile, as shown in figure 3. This behavior is difficult to interpret owing to the presence of several contributions to the emission signal: a contribution from the $^3P_0$ level ($^3P_0 \rightarrow {}^3H_6$ transition overlapping $^1D_2 \rightarrow {}^3H_4$ transition) and the host (see figure 1), both associated with possible ferroelectric-to-antiferroelectric phase transition [28]. The absence of any slow component in the decay suggests however the absence of any afterglow contribution at 77 K in $NaNbO_3:Pr^{3+}$.

The temperature behavior of the $^1D_2 \rightarrow {}^3H_4$ emission of Pr^{3+} has been investigated in the range 300–600 K. The results are plotted in figure 4. The excitation wavelength was 350 nm (i.e. IVCT excitation) for both samples. The luminescence intensity was obtained by integrating the emission area in the range 580–680 nm, after background correction.

The obtained data were reproduced using the model introduced by Struck and Fonger in the case of cross-over to Franck–Condon shifted states [29]. Following this model, the temperature dependence of the emission intensity $I(T)$ is described by

$$I(T)/I_0 = [1 + A \exp(-E/kT)]^{-1}, \qquad (3)$$

where A is close to 10^7 and E is the activation energy from the $4f^n$ state (here $^1D_2$) to its cross-over with the quenching state.

The model showed good concordance with experimental data for $NaNbO_3:Pr^{3+}$ but showed some divergence for $T > 400$ K in the case of $LiNbO_3:Pr^{3+}$. This may be due to the activation of an additional quenching channel in the latter case.

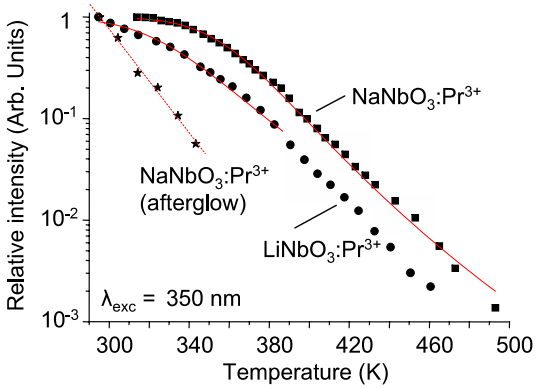

Figure 4. Temperature dependence of the red $^1D_2 \rightarrow {}^3H_4$ emission in $NaNbO_3:Pr^{3+}$ (■) and $LiNbO_3:Pr^{3+}$ (●) excited at 350 nm. The solid line is the fit of the experimental data using equation (3) (see the text). The temperature dependence of the red afterglow in $NaNbO_3:Pr^{3+}$ (stars) is shown for comparison purposes. The dotted line is a single exponential fit of the experimental data.

(This figure is in colour only in the electronic version)

This point was not investigated further in this paper. Using equation (3), the energy barrier between the $^1D_2$ level and the quenching level was estimated at 5700 cm^{-1} for $NaNbO_3:Pr^{3+}$ and at 4100 cm^{-1} (value non-accurate) for $LiNbO_3:Pr^{3+}$.

Oversimplified single coordinate configuration diagrams (see figure 5) were established for $NaNbO_3:Pr^{3+}$ and $LiNbO_3:Pr^{3+}$ on the basis of the optical properties described above. For simplification, the same force constant was used for the parabola and an average energy of 20 500 and 16 500 cm^{-1} was taken for $^3P_0$ and $^1D_2$ levels respectively. The $^3H_4$ ground state is arbitrarily taken at the origin of energies.

It is clear from these diagrams that the IVCT parabola is positioned at a lower energy in $LiNbO_3:Pr^{3+}$ than in $NaNbO_3:Pr^{3+}$. This has a number of consequences.

(1) There is a stronger quenching efficiency of the $^3P_0$ emission in $LiNbO_3:Pr^{3+}$ due to inter-system crossing through the IVCT parabola. This is in agreement with the luminescence spectra displayed in figures 1 and 2.
(2) As the cross-over between $^3P_0$ and the charge transfer state requires thermal activation, the quenching is more efficient at 300 K than at 77 K, as observed experimentally.
(3) At room temperature, the $^1D_2$ emission is partially quenched in $LiNbO_3:Pr^{3+}$ and almost not quenched in $NaNbO_3:Pr^{3+}$, as attested by figure 4 and by the lifetime values reported above for the $^1D_2$ level (27 μs in $LiNbO_3:Pr^{3+}$ against 170 μs in $NaNbO_3:Pr^{3+}$). This partial quenching of the red emission in $LiNbO_3:Pr^{3+}$ is ascribed to the cross-over between the $^1D_2$ level and the IVCT state, followed by non-radiative relaxation to the ground state $^3H_4$.

3.2. *Afterglow properties and possible mechanisms*

The afterglow properties of Pr^{3+}-doped lithium and sodium niobates were investigated as a function of temperature in the range 77–400 K. The irradiation wavelength was 350 nm, corresponding to an excitation in the IVCT band. No afterglow

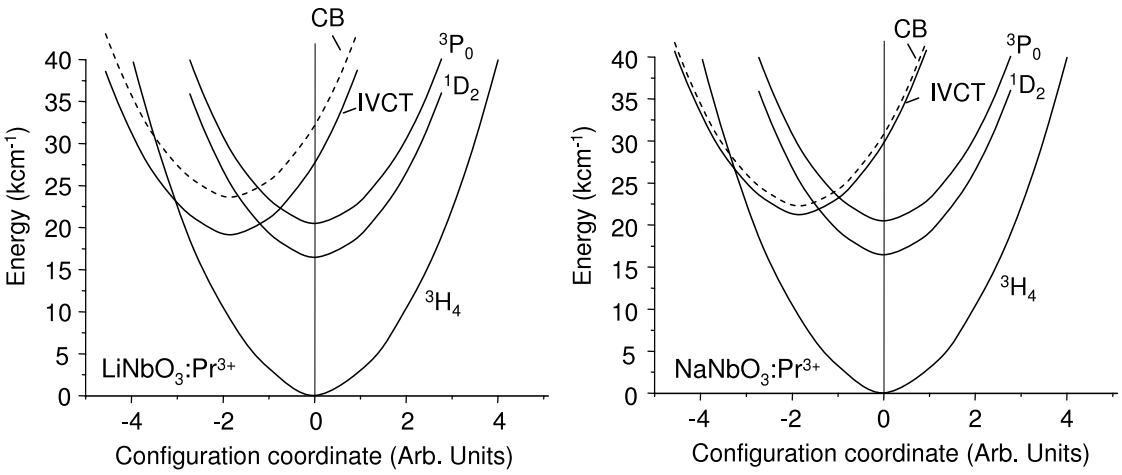

Figure 5. Schematic one coordinate configuration diagrams of Pr^{3+} in $LiNbO_3$ and $NaNbO_3$. The bottom of the conduction band is symbolized as a dotted line.

was detected with our set-up for $LiNbO_3$:Pr^{3+}. In contrast, $NaNbO_3$:Pr^{3+} showed afterglow at $T \geqslant 295$ K but not at $T = 77$ K.

A selection of afterglow spectra is displayed in figure 6. The profile of the emitted afterglow is typical of $^1D_2 \rightarrow {}^3H_4$ transition of Pr^{3+} at room temperature, demonstrating that Pr^{3+} is the recombination center that emits the persistent luminescence.

A similar situation has been observed in $CaTiO_3$:Pr^{3+} [12]. In this compound, an irradiation in the IVCT band results in the transfer of an electron from Pr^{3+} to a nearby Ti^{4+} cation located 3.17 Å from the excited Pr^{3+} [30]. The same process occurs in $NaNbO_3$:Pr^{3+} between Pr^{3+} and a nearby Nb^{5+} ion located at 3.29–3.30 Å from the excited Pr^{3+}.

In $CaTiO_3$:Pr^{3+}, efficient afterglow has been observed at room temperature after irradiation at 380 nm in the IVCT band [12]. This particular situation has been examined by Jia *et al*, who drew conclusions about the possible population of a trapping center from the charge transfer state [11]. Afterglow was then attributed to thermal activation of electrons stored in the trap but no further detail was given about the recombination process with the emitting species.

This model, however, is qualitatively correct and can be transposed to the case of $NaNbO_3$:Pr^{3+}. The proposed afterglow mechanism is therefore the following:

(1) the charge transfer from Pr^{3+} to Nb^{5+} results in a bound exciton consisting of an electron shared among the nearby niobium neighbors adjacent to the excited Pr^{3+} ion;
(2) with thermal activation (i.e. at room temperature), a probability exists that the electron is delocalized at some distance through Nb–O–Nb bridges, thereby increasing the probability for this electron to reach an electron trap (e.g. an oxygen vacancy) and leaving behind a formal Pr^{4+} photo-thermally ionized defect;
(3) a thermal activation releases the electron from the trap according to the Arrhenius equation $P = s\exp(-\Delta E/kT)$ (where P is the probability of thermal de-trapping, s is a frequency factor and ΔE is the trap depth) and permits recombination with the Pr^{4+} defect whose local Coulomb field attracts the electron;
(4) an excited Pr^{3+} ion is formed and glows in the red from the $^1D_2$ level. The determination of the nature of the shallow traps responsible for afterglow is beyond the scope of the present paper and will not be considered here. However, it is reasonable to anticipate the formation of several different kinds of defect centers acting as traps for charge carriers after substitution of Pr^{3+} to Na^+ in $NaNbO_3$:Pr^{3+}, because of charge compensation requirements.

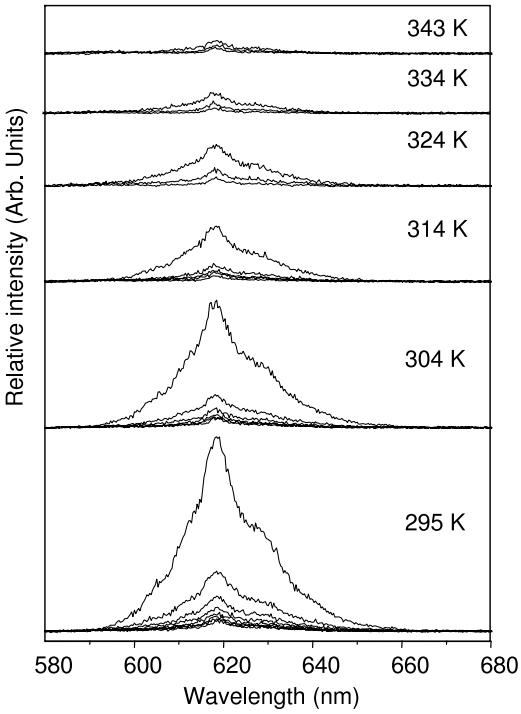

Figure 6. Afterglow spectra of $NaNbO_3$:Pr^{3+} after 1 min irradiation at 350 nm.

Owing to the above model, several comments can be made regarding the afterglow efficiency in $NaNbO_3$:Pr^{3+}.

First, no afterglow is observed at 77 K. This is explained by the fact that the phonon-assisted delocalization (step (2)) and charge de-trapping (step (3)) require thermal activation. The temperature dependence of the afterglow efficiency in the range 77–295 K will be investigated in a future study to clarify this point.

Second, there is a fast exponential decrease of the afterglow efficiency in the temperature range 295–343 K (see figure 4). The rate of this thermal quenching is much higher than the quenching rate of the $^1D_2$ emission in the same temperature range. This indicates that the limiting steps to the afterglow efficiency in $NaNbO_3$:Pr^{3+} are the above steps (2) and (3) again.

The balance between thermal trapping and de-trapping rates that are controlled (at least partly) by the trap depth is obviously a critical parameter. The electron traps in $NaNbO_3$:Pr^{3+} are presumably too shallow to induce efficient afterglow at room temperature and probably brighter afterglow should be observed below 295 K. Thermoluminescence measurements will be carried out to collect information regarding this aspect.

The density of traps and correlatively the probability to find a trap in the nearby environment of a given excited Pr^{3+} ion are also critical. The latter is closely connected with the extension of the electron delocalization in the conduction band after photo-thermal ionization of the Pr^{3+} center.

As reported in section 2, the Nb–O–Nb angles between shared octahedra are closer to 180° in $NaNbO_3$ than in $LiNbO_3$. This property allows a more extended delocalization of the electronic wavefunctions in $NaNbO_3$, as confirmed by a larger Stokes shift of the niobate emission in $NaNbO_3$ than in $LiNbO_3$ (see section 3.1). In our opinion, this difference of electron delocalization contributes to the lower afterglow efficiency in $LiNbO_3$:Pr^{3+} compared to $NaNbO_3$:Pr^{3+}.

4. Conclusion

Pr^{3+}-doped orthorhombic $NaNbO_3$ perovskite is introduced as a new bright red phosphor excitable in the near UV region at room temperature. The photoluminescence properties of this phosphor are described in the frame of the intervalence charge transfer model introduced a few years ago for Pr^{3+}-doped oxidizing lattices containing closed shell d^0 transition metal ions. Afterglow is demonstrated at room temperature in $NaNbO_3$:Pr^{3+} after irradiation in the metal-to-metal charge transfer state and explained by thermally assisted photoionization of the Pr^{3+} ions followed by electron delocalization in the conduction band states.

References

[1] Boutinaud P, Pinel E, Oubaha M, Mahiou R, Cavalli E and Bettinelli M 2006 *Opt. Mater.* **28** 9
[2] Boutinaud P, Putaj P, Mahiou R, Cavalli E, Speghini A and Bettinelli M 2007 *Spectrosc. Lett.* **40** 209
[3] Boutinaud P, Mahiou R, Cavalli E and Bettinelli M 2006 *Chem. Phys. Lett.* **418** 185
[4] Boutinaud P, Mahiou R, Cavalli E and Bettinelli M 2007 *J. Lumin.* **122/123** 430
[5] Boutinaud P, Cavalli E and Bettinelli M 2007 *J. Phys.: Condens. Matter* **19** 386230
[6] Pan Y, Su Q, Xu H, Chen T, Ge W, Yang C and Wu M 2003 *J. Solid State Chem.* **174** 69
[7] Jia W, Xu W, Rivera I, Pérez A and Fernandez F 2003 *Solid State Commun.* **126** 153
[8] Yin S, Chen D and Tang W 2007 *J. Alloys Compounds* **441** 327
[9] Haranath D, Khan A-F and Chander H 2006 *J. Phys. D: Appl. Phys.* **39** 4956
[10] Zhang X, Zhang J, Zhang X, Chen L, Lu S and Wang X-J 2007 *J. Lumin.* **122/123** 958
[11] Jia W, Jia D, Rodriguez T, Evans D-R, Meltzer R-S and Yen W-M 2006 *J. Lumin.* **119/120** 13
[12] Boutinaud P, Pinel E and Mahiou R 2008 *Opt. Mater.* **30** 1033
[13] Lorenzo A, Bausa L-E and Garcia Sole J 1995 *Phys. Rev.* B **51** 16643
[14] Lorenzo A, Jaffrezic H, Roux B, Boulon G, Bausa L-E and Garcia-Sole J 1995 *Phys. Rev.* B **52** 6278
[15] Raevski I-P and Prosandeev S-A 2002 *J. Phys. Chem. Solids* **63** 1939 and references therein
[16] Megaw H-D 1954 *Acta Crystallogr.* **7** 187
[17] Piramidowicz R, Prackat I, Wolinski W and Malinowski M 2000 *J. Phys.: Condens. Matter* **12** 709
[18] Koepke Cz, Wisniewski K, Dyl D, Grinberg M and Malinowski M 2006 *Opt. Mater.* **28** 137
[19] Blasse G and De Haart L-G-J 1986 *Mater. Chem. Phys.* **14** 481–4
[20] Grigorjeva L, Millers D, Trepakov V and Kapphan S 2004 *Ferroelectrics* **304** 117
[21] Chen C-Y, Chen J-C and Chia C-T 2007 *Opt. Mater.* **30** 393
[22] Bhatt R, Kar S, Bartwal K-S and Wadhawan V-K 2003 *Solid State Commun.* **127** 457
[23] Gryk W, Kuklinski B, Grinberg M and Malinowski M 2004 *J. Alloys Compounds* **380** 230
[24] Capobianco J-A, Raspa N, Monteil A and Malinowski M 1993 *J. Phys.: Condens. Matter* **5** 6083
[25] Malinowski M, Garapon C, Joubert M-F and Jacquier B 1995 *J. Phys.: Condens. Matter* **7** 199
[26] Guyot Y, Moncorgé R, Merkle L-D, Pinto A, McIntosh B and Verdun H 1996 *Opt. Mater.* **5** 127
[27] Pinel E, Boutinaud P, Bertrand G and Mahiou R 2004 *Proc. SPIE* **5250** 444
[28] Darlington C-N-W and Megaw H-D 1973 *Acta Crystallogr.* B **29** 2171
[29] Struck C-W and Fonger W-H 1971 *J. Appl. Phys.* **42** 4515
[30] Boutinaud P, Pinel E, Dubois M, Vink A-P and Mahiou R 2005 *J. Lumin.* **111** 69